Energy 356 (2026) 141149

Contents lists available at ScienceDirect

Energy

journal homepage: www.elsevier.com/locate/energy

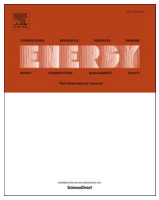

Evaluation of thermal energy storage for medium-low temperature applications: Comparison of commercial solutions with a xylitol-based prototype

Miguel Navarro *, Ana Lázaro, Mónica Delgado

Aragón Institute for Engineering Research (I3A), Thermal Engineering and Energy Systems Group, University of Zaragoza, Agustín de Betancourt Building, C/María de Luna 3, 50018, Zaragoza, Spain

ARTICLE INFO

Keywords:
Xylitol
Thermal energy storage
Latent heat
Commercial systems
Prototype

ABSTRACT

In recent years, thermal energy storage (TES) has become a promising and popular technology for energy storage. Among the different technologies, this work focuses on latent heat thermal energy storage (LHTES) system, specifically it assesses the potential of xylitol as phase change material (PCM) in TES systems for low-medium temperature applications. Xylitol, a sugar alcohol with stable supercooling, has a high latent heat (240 J/g), high energy storage density (1.45 kg/l), and a melting temperature of 92 °C. However, stable supercooling and low crystallization rate limits its practical application. Therefore, a laboratory-scale prototype working in the 70-100 °C range has been proposed and experimentally characterised that uses a seeding and shearing technique to mitigate this supercooling and accelerate crystallization, thereby increasing the thermal energy discharge power. The study compares this lab-scale prototype with four leading commercial solutions in terms of both materials and systems. Moreover, the methodology developed in the framework of IEA SHC Task 58 for TES system comparison in terms of energy density and power is applied. The results show the xylitol prototype has higher normalized power values than other experimental systems analysed in the framework of IEA SHC Task 58, reaching energy densities of up to 40.8 kWh/m^3 system-wise in an optimized configuration. The study concludes that stirred TES prototype with xylitol is a competitive alternative to current commercial solutions.

1. Introduction

In the path to decarbonising society, renewable energy sources play an important role in phasing out different energy sources that contribute to global warming and contamination of the planet, such as carbon. However, these renewable energy sources are highly dependent on climate, which desynchronizes generation and demand. As such, energy storage is needed to match generation and demand. Energy storage integration also increases the efficiency and reliability of the energy systems. Excess energy generated at one moment in time can be stored and used when it becomes necessary, which optimizes the system by reducing the need for oversizing capacity production and allowing for a more consistent operation.

Among the different energy storage technologies currently available, Thermal Energy Storage (TES) stands out as a suitable solution for applications where heat and cold are required, as industrial processes and polygeneration systems [1], [2]. TES can also be coupled with technologies, such as heat pumps, extending its role beyond purely thermal applications. TES technology is becoming increasingly important in the industry sector, although more solutions are becoming commercially available for residential use. TES systems can be divided into three main technologies: sensible heat, thermochemical and latent heat.

Although sensible heat is the most mature, its low energy density limits compactness [1], [2], [3]. Conversely, thermochemical storage offers high density but remains in a research stage [3], [4]. Latent heat thermal energy storage (LHTES), based on the phase change of a material, provides a favourable compromise by combining high energy density with the ability to store and release heat at nearly constant temperature, making it especially attractive for a wide range of thermal applications.

In LHTES systems, phase change materials (PCMs) such as paraffins, molten salts or sugar alcohols are used to store energy through solid–liquid phase transitions [5], [6], [7]. Molten salts are widely

This article is part of a special issue entitled: ICP2025 - Invitation Only published in Energy.

* Corresponding author.
E-mail address: miguel.navarro@unizar.es (M. Navarro).

https://doi.org/10.1016/j.energy.2026.141149
Received 2 February 2026; Received in revised form 31 March 2026; Accepted 23 April 2026
Available online 7 May 2026

Nomenclature

Variables and abbreviations

$\overline{c_{pHTF}}$	Average specific heat of the HTF, in J/kg·K
EC	Energy Capacity, in J
$ED_{with\ ins}$	Energy Density of the insulated TES
$ED_{no\ ins}$	Energy density of the non-insulated TES
Δh_{PCM}	Enthalpy difference of the PCM, in J/g
Δh_{sys}	Enthalpy difference of the TES system, in J/g
ΔT	Temperature difference between the PCM and the ambient, in °C
HTF	Heat Transfer Fluid
HVAC	Heating, Ventilation and Air Conditioning
LHTES	Latent Heat Thermal Energy Storage
$\dot{m}$	Mass flow of the HTF, in kg/s
m_{PCM}	Mass of the PCM, in g
m_{sys}	Mass of the TES system, in g
PCM	Phase Change Material
SoC	State of Charge
τ	Torque of the mechanical stirrer, in N·m
T_{amb}	Ambient temperature, in °C
t_{end}	end time of the experiment, in seconds
TES	Thermal Energy Storage
T_{inlet}	Inlet temperature of the HTF in the system, in °C
T_{outlet}	Outlet temperature of the HTF in the system, in °C
T_{ref}	Reference temperature of the system, in °C
t_{start}	Starting time of the experiment, in seconds
$\overline{T}_{sys}$	Average temperature of the system, in °C
Q_{norm}	Normalized energy of the power, in Joules
$\dot{Q}$	Instantaneous thermal power of the system, in Watts
$\dot{Q}_{int}$	Instantaneous thermal power of the system, in Watts
$\dot{Q}_{loss}$	Thermal losses of the system, in Watts
$\dot{Q}_{norm}$	Normalized thermal power, in W/m^3·K
Q_{norm}	Normalized thermal energy, in J/m^3·K
$\overline{\dot{Q}^{norm}_{energy}}$	Normalized mean value of the power, energy-based, in W/(m^3·K)
$\overline{\dot{Q}^{norm}_{time}}$	Normalized mean value of the power, time-based, in W/(m^3·K)
$\dot{Q}_{tot}$	Heat difference between coil inlet and outlet, in Watts
UA	Thermal losses heat transfer coefficient of the system, in W/K
V	Sum of the volume of the PCM and HTF, in m^3
V_{tot}	Total volume of the TES system, in m^3
$V_{no\ ins}$	Volume of the TES system with no insulation, in m^3
ω	Stirring velocity of the mechanical stirrer, in rad/s
$\dot{W}_{stir}$	Mechanical power input from by the stirrer, in Watts

implemented in concentrated solar power plants, while other PCMs are used for residential, commercial and industrial uses, including HVAC systems and waste heat recovery [3], [5], [6]. The performance of LHTES systems depends not only on the thermophysical properties of the PCM, but also on operational conditions (inlet temperature, heat transfer fluid (HTF) flow rate) and system-specific characteristics such as geometry and size. Consequently, a methodology is required to allow a fair comparison between different storage concepts and scales.

Various studies have already addressed the characterisation PCM-based TES systems. Larrinaga et al. [8] studied a rectangular LHTES system with fourteen different aluminium plates, filled with RT60, at different mass flow rates and operating temperatures. Larrinaga et al. found that the operating temperatures affected the required time to fully charge and discharge the system, and used the temperature difference between the inlet and the interior of the system to analyse the change of the charging times of the system at the different operating conditions. Dolado et al. [9] characterised a PCM-air TES unit, both experientially and numerically. This work mainly uses the power versus time curves obtained from the simulation to observe the effects on power by changing different parameters, such as the PCM enthalpy or the phase change temperature.

More recently, Rinaldi et al. [10] used a theoretical model of a tank with an emulsion with PCM to be used in the study of a district heating system. This study compared several PCM emulsion tanks of different configurations with a water tank to be used as TES, showing the stored energy of the water tank and the hourly demand power curve. However, the effect of using the PCM emulsion tank was shown only in the hourly mass flow curve, and the thermal power curve was not explicitly shown. The experimental data for the PCM emulsion tank were taken from Delgado et al. [11], which shows the UA heat transfer coefficient data. Luo et al. [12] studied the performance of a molten salt tank with air as HTF for system discharge and electrical resistance for charging. This LHTES system is used to heat water through an air-water finned tube exchanger in discharge experiments conducted at constant power. This study showed the average power of the tests under different flow rates and compared other energy storage systems found in the literature. Yang et al. [13] studied the behavior of a cascade storage system using erythritol, another sugar alcohol different from xylitol, in one of the phases. This study shows the power curves in both constant and variable flow rate tests to maintain the outlet temperature above 60 °C.

In general, the characterisation of storage systems consists of obtaining both energy and power curves over time, at different operating conditions. These studies, together with others found in the literature ([11], [14], [15], [16]), highlight the difficulties to obtain different characterization parameters of LHTES systems, and the need for a standard methodology for evaluating energy density and power, in order to evaluate some systems compared to others, and propose more suitable TES system designs.

The work of König-Haagen et al. [17], following the previous study of Lazaro et al. [18], proposes a methodology that uses of normalized power and energy curves for comparing different storage systems. This work uses the work of IEA SHC Task 58/Annex 33 [17] and presents a comparison of 11 different systems.

In this context, the present study focused on a laboratory-scale LHTES system based on a stirred tank with an internal coil heat exchanger. This type of system is a robust and economical solution for energy storage. Along with this system, xylitol was chosen as the PCM. Xylitol is a sugar alcohol that has good characteristics for use as a storage material (high phase change enthalpy and high density [19], [20], [21], [22], [23], [24]). However, as shown in previous work and literature, xylitol also exhibits supercooling and low crystallization rate [21], [24], [25], [26]. A stirred tank allows for the simple incorporation of the seeding and shearing technique, which is used to activate and accelerate crystallization, thereby avoiding these drawbacks. Several studies have investigated the use of xylitol as a phase change material in thermal energy storage systems. Piquard et al. [27] studied xylitol in a bubbling system and demonstrated the viability of xylitol as a phase-change material despite the difficulty in inducing crystallization. In a subsequent work [28], the same authors applied this approach to a shell-and-tube configuration, analyzing the evolution of stored energy and temperature during the crystallization process. Anish et al. [29] investigated a coil-equipped tank using xylitol. Interestingly, no specific strategy was implemented to trigger crystallization, allowing the material to remain in a metastable supercooled state, albeit at lower operating temperatures. In contrast, Navarro et al. [30] compared a bubbling system with a jacketed stirred tank. While power curves were

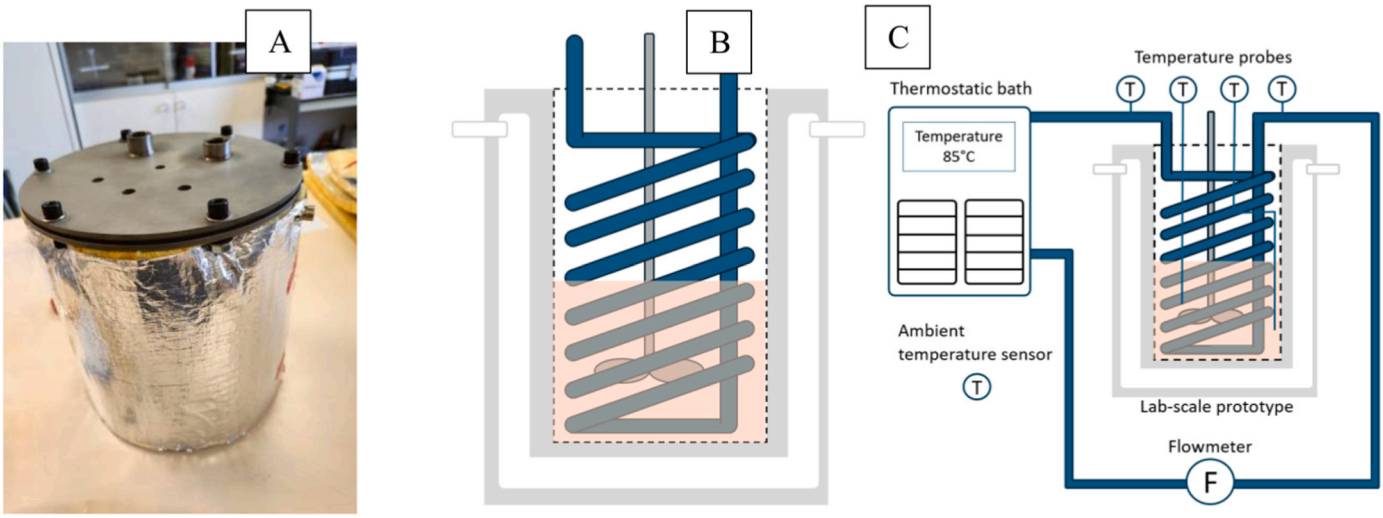

Fig. 1. Laboratory-scale stirred tank TES prototype using xylitol as PCM, with an inlet for seeding. A) Photo of the body of the tank. B) Scheme of the tank, showing the body, the coil, the jacket and the stirrer. C) Experimental set-up Schematic.

reported for the bubbling configuration, no such analysis was provided for the stirred system.

The present work introduces a stirred tank equipped with an internal heat exchange coil, representing a novel configuration. This design is expected to enhance heat transfer performance through the combined effect of mechanical agitation and improved heat exchange efficiency associated with the internal coil, as opposed to conventional jacketed configurations.

The objective of this work is to characterise the performance of the lab-scale xylitol-based prototype to compare it with commercially available systems (in terms of energy density, thermal power or price) and those reported in the IEA SHC Task 58/Annex 33. The prototype is characterized using the methodology proposed by the IEA Task Group itself, which addresses the standardization of both instantaneous thermal power and average thermal power which was published in the paper by König-Haagen et al. [17], as well as the energy density defined in the IEA SHC Task 58/Annex 33 report [31]. To characterise the laboratory-scale prototype, tests are first carried out under different operating conditions at a constant inlet temperature.

2. Methodology

2.1. Lab-scale prototype characteristics

In this work, 99%purity xylitol from Thermo Scientific was used as PCM. Xylitol is a sugar alcohol with a phase change temperature of 92 °C and a phase change enthalpy of 240 J/g [21], [23], [32]. The seeding material to trigger crystallization were xylitol seeds, with a diameter of 300-400 μm. These seeds are obtained by sieving chinks of fresh xylitol, directly from the Thermo Scientific batch.

The prototype designed for this study consists of a jacketed cylindrical steel tank that integrates an internal coil and a mechanical agitation system. The main body has an internal diameter of 150 mm and an internal height of 230 mm. The thermal insulation is glass wool, with a thickness of 20 mm. With the glass wool as insulation, the height of the system is 290 mm, and an external diameter of 245 mm with the insulation and the jacket, so the external volume of the system is 0.0136 m^3 (13.6 L). Without insulation, the height of the system is reduced to 270 mm, and the external diameter to 205 mm, corresponding to a volume of 8.91 L. The system was designed with a temperature control system to utilize the jacket, but ultimately only the coil was used for temperature control. However, the complete volume of the prototype with the jacket will used in some of the system characteristics that appear in the results section.

For heat exchange, an 11-turn copper coil made of 8 mm internal diameter pipe is used with a helical diameter of 110 mm. The system uses 2.5 kg of xylitol as PCM. Due to the stable supercooling of this sugar alcohol, the prototype incorporates a mechanical stirrer (IKA 60 control mechanical stirrer) to implement the shearing technique. This technique is used in the study by Delgado et al. [25], and in the previous work of the authors of this article [30]. The stirrer is positioned along the central axis of the tank. This configuration allows crystallization to be activated and promoted in a controlled manner during discharge. As xylitol presents both supercooling and a low crystallization rate, a stirrer is added. This stirrer, in combination with a seeding technique, both activates and promotes crystallization on xylitol. However, the space of the stirrer was not considered for the calculation of the volume or the energy capacity. Seeding is performed through one of the upper holes of the tank.

The system's thermal management is carried out by means of a thermostatic bath (Julabo Corio CP 1001F) that circulates thermal oil (Julabo H10) through the coil as HTF. To monitor the process, two 4-wire Class B Pt100 sensors have been installed inside the tank to measure the PCM temperature over the stirrer position and between the coil and the wall of the tank. Another two 4-wire Class B Pt100 sensors are placed at the coil inlet and outlet. These sensors have a measurement uncertainty of 0.21 °C. The HTF flow rate is measured by a Trigear TC008A2212100 positive displacement oval gear flowmeter with a ±0.5% precision, thus allowing the instantaneous thermal power of the system to be calculated accurately. A Type-T thermocouple is used to measure ambient temperature, with an uncertainty of 0.5 °C. Fig. 1A shows the body of the system, Fig. 1B shows a scheme of the tank, and Fig.1C shows the experimental set-up schematic.

The PCM used for this system is xylitol. Xylitol is a sugar alcohol, with a phase change temperature of 92 °C, a density of 1.45 g/cm^3 and a phase change enthalpy of 240 kJ/kg [19], [21], which gives it an energy density of 97 kWh/m^3. This prototype is not well optimized for a TES system, and improvements could be made to obtain higher energy density or thermal power.

2.2. Characterization of the laboratory-scale TES prototype

2.2.1. Discharge experiments

The discharge experiment was executed as follows: first, the xylitol is melted, maintaining an internal temperature of 105^0C. It was then supercooled down to a stable supercooled state at the test temperature of 85^0C. Once a steady state had been reached at that temperature, 12.5 mg

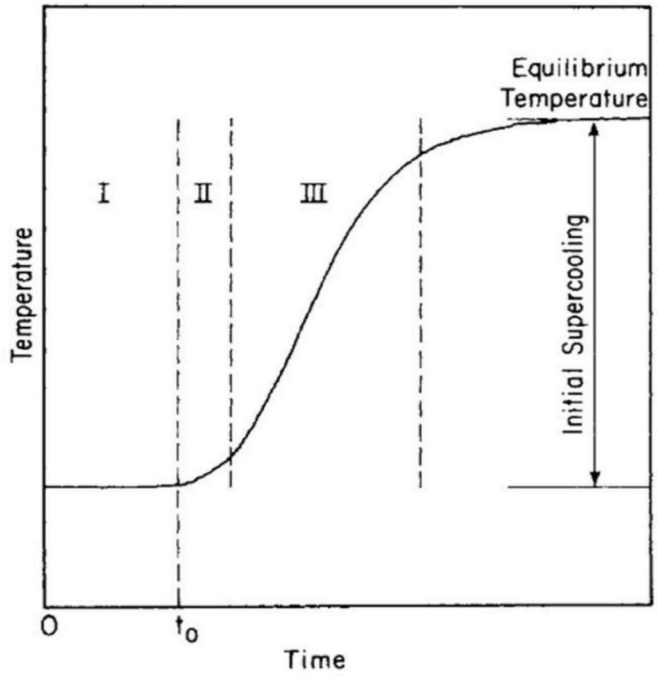

Fig. 2. Temperature evolution of the system in a crystallization experiment, provided by Omran and King [33].

of seed was added and stirred at 500 rpm. These seeds are obtained by sieving xylitol chunks from Thermo Scientific at 99% purity; and had a diameter between 300 and 400 μm. The temperature was chosen as 85 °C because it is low enough to allow rapid crystallization of xylitol without incurring significant energy loss [25], [30]. The stirring speed was selected as 500 rpm because it can accelerate crystallization [26], while the seed mass fraction was kept consistent with that used in the work of Delgado et al. [25].

Of these three operating conditions (initial temperature, seed quantity and stirring speed), temperature is expected to have the greatest influence on crystallization time, as seen in the literature [20], [26]; and on instantaneous thermal power, due to recalescence and the temperature difference between the inlet and the interior. It is expected that tests with greater supercooling will have a higher maximum thermal power, as recalescence will increase the interior temperature of xylitol to 92 ^{0}C, increasing the temperature difference between interior and inlet. However, supercooling causes part of the energy stored in the material to be used in recalescence, so greater supercooling means less energy discharged. Navarro et al. [30] argued that due to recalescence, part of the latent heat stored in xylitol is used to heat the supercooled liquid to the phase change temperature. They also argue that, once the phase change is complete, energy continues to be transferred from the solid to the HTF due to the difference in their temperatures. Therefore, the theoretical energy discharged is less than the latent heat of the system, because the specific heat of the solid is lower than the specific heat of the liquid.

Fig. 2 shows the temperature evolution of a supercooled system during the crystallization process. Initially, the temperature remains constant while the material stays in a metastable liquid state. Once crystallization is triggered, the release of latent heat leads to a rapid increase in temperature until it reaches the crystallization temperature. After complete solidification, the material, now fully solid, continues to release sensible heat, causing the system temperature to gradually decrease until thermal equilibrium with the surroundings is reached [30], [33], [34].

To calculate the instantaneous heat output, an energy balance is carried out for the system, as shown in equations (1)–(4).

$$\dot{Q}_{int} = \dot{Q}_{tot} + \dot{W}_{stir} - \dot{Q}_{loss} \quad \text{Eq. 1}$$

$$\dot{Q}_{tot} = \dot{m} \cdot \overline{c}_{pHTF} \cdot (T_{inlet} - T_{outlet}) \quad \text{Eq. 2}$$

$$\dot{W}_{stir} = \tau \cdot \omega \quad \text{Eq. 3}$$

$$\dot{Q}_{loss} = UA \cdot \Delta T; where\ \Delta T = \overline{T}_{sys} - T_{amb} \quad \text{Eq. 4}$$

The total heat transfer rate $\dot{Q}_{tot}$ [W], is calculated as the product between the mass flow rate $\dot{m}$ [kg/s], the average specific heat of the HTF $\overline{c}_{pHTF}$ [J/kg·K] and the temperature difference between the inlet T_{inlet} and the outlet T_{outlet} [°C or K]. $\dot{W}_{stir}$ represents the mechanical power input from by the stirrer, calculated as the product of the torque τ [N·m] and the stirring velocity ω [rad/s]. Thermal losses, $\dot{Q}_{loss}$ [W] are estimated using the overall heat losses coefficient UA [W/K], multiplied by the temperature difference between the average system temperature $\overline{T}_{sys}$ and the ambient temperature T_{amb} [°C or K].

The UA coefficient is calculated under steady state conditions reached at the end the experiment. At this stage, no the heat is exchanged between the xylitol and the HTF. Therefore, the temperature difference between the inlet and outlet of the coil is attributed to the thermal losses and the mechanical work done by the stirrer due to friction with the solidified PCM.

2.2.2. Energy capacity and energy density of the system

The correct characterisation of the system uses both the energy storage capacity and the energy storage density of the system. The IEA SHC Task 58/Annex 33 proposes a definition for both the energy storage capacity and density In the final report of this Task [31], the stored energy capacity is proposed as the sum of the storage capacities of both the PCM and the mass of the system itself, defined according to Eq. (5).

$$EC = m_{PCM} \cdot \Delta h_{PCM} + m_{sys} \cdot \Delta h_{sys} \quad \text{Eq. 5}$$

Where EC is the energy capacity of the system, m_{PCM} is the mass of the PCM, m_{sys} is the mass of the system, and Δh is the enthalpy variation of all components and materials in the storage system determined over the operating temperature range. This characterisation takes into account the sensible heat storage of the system, not just the PCM, but the system material itself. A deep understanding of the thermophysical properties of the PCM, such as latent heat and specific heat, as well as the mass and heat capacity of the materials composing the system, is needed for an accurate estimation of stored energy; as all of these parameters introduce uncertainties into the energy balance. For instance, xylitol exhibits a latent heat in the range of 220–270 J/g [32], [35], [36], highlighting the variability reported in the literature. To address this issue, specific measurement procedures have been proposed within Task SHC42 ECES29 to ensure a more reliable determination of latent heat and melting temperature. In addition, when sensible heat contributions are considered, accurate representation of the system temperatures becomes important. However, determining a representative average temperature is challenging due to temperature gradients within the system. Different components may operate at significantly different temperatures. For example, the insulation is typically at a lower temperature than the heat exchanger, which is in direct contact with the PCM. Similarly, when the PCM stores energy in the form of sensible heat, defining its exact average temperature is difficult, further contributing to uncertainty in the calculated stored energy.

For the purposes of this study, since the initial and final temperatures of the test are considered to be the same, the sensible heat stored in the system components is not taken into account. Although energy capacity should be reduced due to supercooling [30], this subcooling will not be taken into account in this study when calculating the energy capacity of the system.

On the other hand, characterising the system using energy density poses a certain problem when choosing the volume of the system. Ac-

cording to the IEA SHC Task 58/Annex 33 work [31], both volumes with and without insulation can be used to characterise a storage system. Therefore, two different energy densities appear in this work, calculated according to Eq. (6) and Eq. (7).

$$ED_{with\ ins} = EC\ /V_{tot} \quad \text{Eq. 6}$$

$$ED_{no\ ins} = EC/V_{no\ ins} \quad \text{Eq. 7}$$

Where ED is the energy density, EC is the Energy capacity of the system, and V is the considerate volume, with and without insulation.

As mentioned in the previous section, the supercooling reduces the available energy due to the difference between the solid and liquid specific heats. Theoretically, the lab scale prototype uses 2.5 kg of xylitol, so it can store up to 600 kJ of energy, corresponding only for the latent heat stored energy. For the energy available at the supercooled state, the theoretical energy is calculated through Eq. (8):

$$EC = m\cdot\left[\Delta h_{PCM} - c_{p_{xyl}}^{liq}\cdot\left(T_{melt} - T_{sup}\right) + c_{p_{xyl}}^{sol}\cdot\left(T_{melt} - T_{sup}\right)\right] \quad \text{Eq. 8}$$

Where m is the mass of the PCM, Δh_{PCM} is the latent heat of the PCM, in kJ/kg, $c_{p_{xyl}}^{liq}$ and $c_{p_{xyl}}^{sol}$ are the specific heats of the solid and liquid phases of the PCM, in kJ/kg·K, T_{melt} is the melting point of the PCM and T_{sup} is the supercooling temperature.

2.2.3. Normalized thermal power

In TES systems, instantaneous power varies throughout the charging and discharging process, remaining consistently in a transient state. This complicates its characterization; while this instantaneous power can be determined by evaluating the mass flow rate of the heat transfer fluid (HTF) and the temperature differential (or temperature lift) between the inlet and outlet as it flows through the system's heat exchanger, its time-dependent evolution and magnitude depend on several parameters. These include the temperature difference between the HTF inlet and the material's phase change temperature, the system's State of Charge (SoC), and its specific size and geometry, among others. Thus, in the work of König-Haagen et al. [17], the difficulty of comparing different storage systems was discussed, given that both thermal power and energy depend on the operating conditions of the system, as well as its geometry and the materials it is made of. Normalizing the power with volume and temperature difference is proposed to assess the systems. In this article, normalized power is defined according to Eq. (9). This study also compares both the initial temperature of the system and the melting point of the PCM as the reference temperature. However, in this case only the initial temperature was considered.

$$\dot{Q}_{norm} = \frac{\dot{Q}}{V\cdot\left(T_{inlet} - T_{ref}\right)} \quad \text{Eq. 9}$$

Where $\dot{Q}_{norm}$ is the normalized thermal power, $\dot{Q}$ is the instantaneous thermal power of the system, V is calculated as the sum of the volume of the PCM and the volume of the HTF that flows inside the system, T_{inlet} is the inlet temperature of the HTF in the system, and T_{ref} is the reference temperature of the system, which can be either the initial temperature of the system, or the melting point of the PCM. It is noted that, even though this work comes from the IEA SHC Task 58/Annex 33, the volume definition is different from the previous definitions, shown in Section 2.2.2.

The mean normalized thermal power is also proposed by König-Haagen et al. [17]. This characterization of the system could allow to compare different TES systems with just one parameter, instead of comparing them using thermal power curves, allowing for a quick comparison. The calculation of the mean normalized power, time and energy based is shown in Eq. (10) and Eq. (11), respectively.

Table 1
Characterization parameters of the lab scale prototype and the optimize TES system.

System	EC [kWh]	V_{Tot} [l]	$V_{no\ ins}$ [l]	$ED_{with\ ins}$ [kWh/m^3]	ED_{no_ins} [kWh/m^3]
Lab-scale prototype	0.16	13.60	8.91	11.82	18.04
Optimized prototype	0.29	7.08	4.43	40.83	65.25

$$\overline{\dot{Q}_{time}^{norm}} = \frac{\int_{t_{start}[s]}^{t_{end}[s]}\dot{Q}_{norm}\cdot dt}{\left(-t_{start}\right)} \quad \text{Eq. 10}$$

$$\overline{\dot{Q}_{energy}^{norm}} = \frac{\int_{t_{start}}^{t_{end}}\dot{Q}_{norm}\cdot\dot{Q}_{norm}\ dt}{Q_{norm}} \quad \text{Eq. 11}$$

Where $\overline{\dot{Q}_{time}^{norm}}$ is the normalized mean value of the power, time-based; $\overline{\dot{Q}_{energy}^{norm}}$ is the normalized mean value of the power, energy-based; $\dot{Q}_{norm}$ is the normalized instantaneous power of the system, Q_{norm} is the normalized energy, calculated as the integral of the instantaneous power of the system; t_{start} is the starting time of the experiment and t_{end} is the finish time of the experiment. The end of the experiment is reached when 95% of the energy in the experiment has been exchanged.

2.3. Commercial systems

In this work, four different commercially available TES systems are chosen to be studied and compared to the lab-scale prototype described above and developed by the authors. The parameters for comparison are taken from product specifications available on their respective websites, as well as articles authored by the companies' founders or published research on these products, or through discussions with technical support. These four commercial solutions are found in Sunamp, Cowa Thermal Solutions, kraftBoxx, and Cartesian [37], [38], [39], [40].

The comparison of commercially available solutions is conducted in two parts. First, the phase change materials used in each system are identified, and their properties are taken from either the websites or the literature. The properties considered for the comparison of the different PCMs include the type of material, melting point, phase change enthalpy, and energy density. The second part of this work studies the systems themselves. One system from each company is selected and compared to the lab-scale prototype. The systems are assessed based on working temperature, energy capacity, thermal power, energy losses, and price. Energy density is calculated by dividing the system's energy storage capacity by its external volume, taking into account the system's insulation.

3. Results

3.1. Lab-scale prototype

3.1.1. Prototype characterization

As mentioned in Section 2.1, The lab-scale prototype consists mainly of a jacket and coil stirred tank, even though only the coil is used for the study of the system; where the coil is submerged in 2.5 kg of xylitol. Table 1 shows the energy capacity and density of the lab-scale prototype and the optimized system, following the methodology proposed in section 2.2.2. Using Eq. (8) and considering 240 kJ/kg as the latent heat of xylitol, 2.6 and 1.4 the specific heat of the liquid and solid phases, and 92 °C as the melting point, the theoretical energy available is 579 kJ. The experimental available power, calculated by integration of the discharged thermal power in section 3.1.3, shows good agreement with the theoretical value. For simplicity, this theoretical value is used through the next section as the available power. It should be noted that

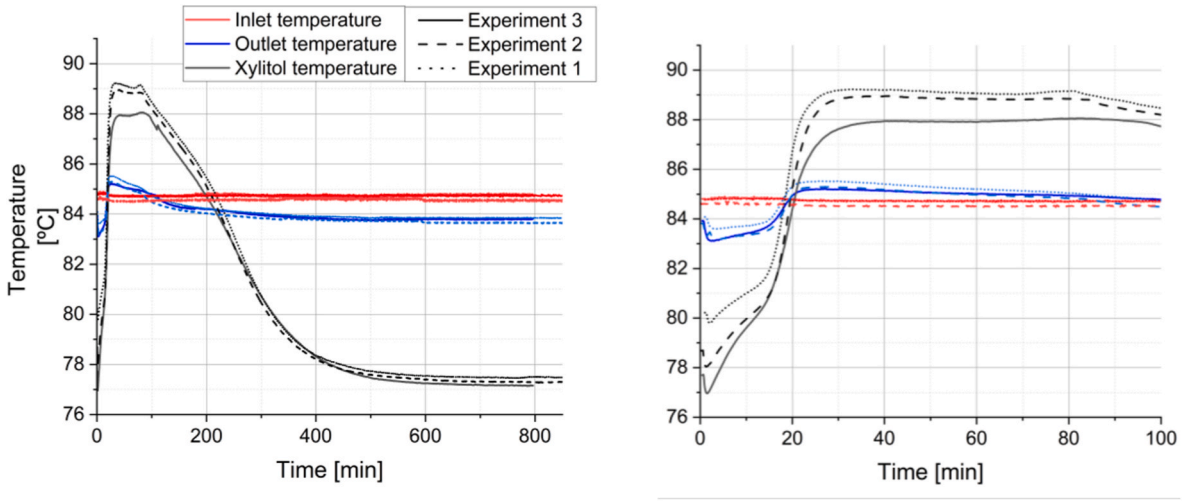

Fig. 3. Temperature evolution of the system. A) Temperature evaluation through the system. B) Temperature evolution at the start of the experiment.

the proposed system requires an external component for proper operation, which has not been included in the volume calculation; however, incorporating this component into a consistent volumetric definition remains challenging. As such, only the body of the tank is considered for the volume calculation. With a volume of 13.6 L, its energy capacity is 11.82 kWh/m^3. With no insulation, the volume is 8.91 L, and the energy density changes to 18.04 kwh/m^3.

In an optimized configuration, the xylitol occupies the entire available internal volume, corresponding to a mass of 4.5 kg. This optimized laboratory prototype does not use a jacket, so both its external diameter and height are reduced. With insulation and no jacket, the external diameter is reduced from 245 to 190 mm, while the height is reduced from 290 to 250 mm, resulting in a cylinder with a volume of 7.08 L.

Considering the supercooling to 85 °C, the energy available jumps to 1042 kJ. Thus, the system's storage capacity would increase to 40.83 kWh/m^3. The external volume of the optimized laboratory scale prototype is calculated as a cylinder with a diameter of 155 mm and a height of 235 mm, making the total volume 4.43 L and the energy density 65.25 kWh/m^3. For both cases, the energy density is higher if insulation is not taken into account. Due to the lack of data from some manufacturers, the characterisation volume used for the comparison will be the total volume of the system, including insulation.

3.1.2. *Temperature evolution*

Fig. 3 shows the evolution of the average tank temperature for three different tests of the prototype. These tests were carried out in accordance with the methodology described in section 2.2.1, under the same conditions: an inlet temperature of 85 °C, a stirring speed of 500 rpm and a seed quantity of 12.5 mg.

Fig. 3A shows the complete temperature evolution of the three experiments, while Fig. 3B focuses on the beginning of the test. As observed in Fig. 3B, in contrast with Fig. 2, where the initial temperature of the experiment remains constant, an initial temperature drop occurs at the start of the experiment. This behaviour is attributed to the initial lack of thermal homogeneity within the tank. As agitation starts, temperature gradients are reduced, leading to a transient decrease in the measured temperature. However, before the system temperature reaches equilibrium, a more pronounced temperature increase is observed, associated with the recalescence phenomenon, which increases the material temperature due to the release of latent heat. As in Fig. 2, once the crystallization temperature is reached, the temperature remains nearly constant until the end of the phase change. After complete solidification, the xylitol, now in solid form, gradually cools down until the system returns to steady-state conditions.

3.1.3. *Discharging thermal power*

Three different test repetitions of the lab-scale prototype are shown

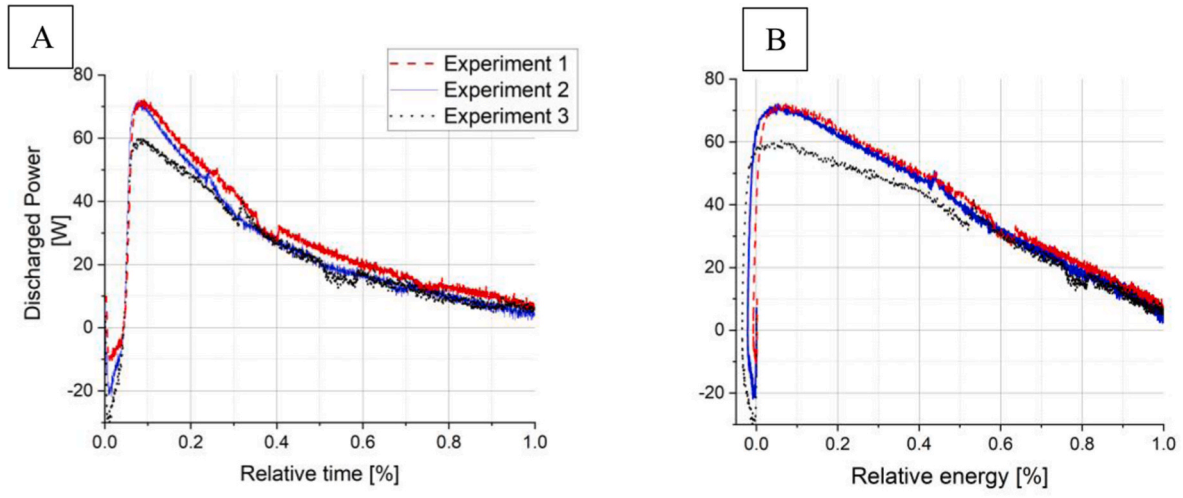

Fig. 4. Discharged power of the lab-scale prototype. A) Discharged power vs. Relative Time. B) Discharged power vs. Relative Energy.

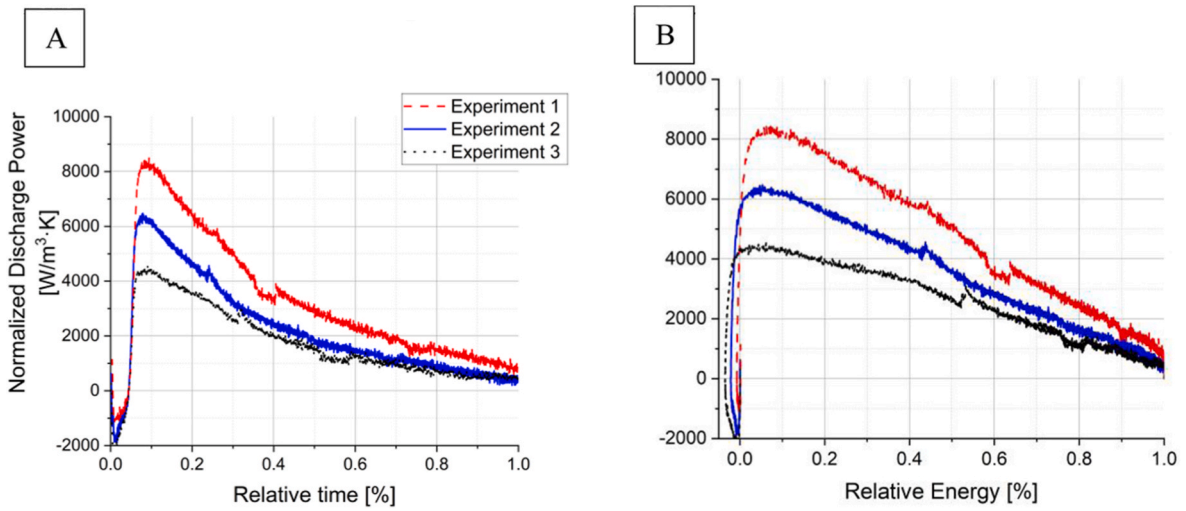

Fig. 5. Normalized discharged power of the lab-scale prototype. A) Normalized Power vs relative time. B) Normalized Power vs Relative energy.

in Fig. 4. As mentioned in section 2.2.1, these tests were conducted under the same operating and initial conditions: the inlet temperature of the test was 85 ^{0}C, the stirring velocity was 500 rpm, and the seed mass used to activate crystallization was 12.5 mg. The prototype was tested following the methodology on Section 2.2.1.

Fig. 4 shows the immediate power against relative time (A) and against relative energy (B), taking as a reference the moment when 95% of the energy has been discharged. The use of relative time and relative energy to show power results was taken from the literature [17], [41]. This method to present the data is maintained through this work. The discharged power increases at the beginning of the test and then decreases as the test progresses. The initial increase in power up to the peak is due to recalescence, which causes the internal temperature to rise to the phase change temperature (92 ^{0}C). This increase in internal temperature also causes the outlet temperature of the coil to rise, which translates into an increase in thermal power.

A sharp drop in power to negative values can also be observed, which quickly changes to positive power and towards the maximum power. These negative values make the energy negative at the start of the test, causing the power curve in graph B of Fig. 4 to initially shift to the left. It is noted that there is no temperature uniformity in the prototype, as there is a deviation in the temperature of the xylitol in the centre of the system and the xylitol near the wall. This non-homogeneity is reduced when agitation begins, causing a drop in the outlet temperature of the system. These negative values are also associated with a poor representation of thermal losses, which may drop the initial power values even lower.

3.1.4. Normalized discharging thermal power

The normalisation of the instantaneous power curves in section 3.1.3 is obtained by following the methodology in section 2.2.3. The volume used is 0.00192 m^3, and the internal temperature is calculated as the average of the probe temperatures. The result of this normalisation is shown in Fig. 5.

It can be seen in the normalisation that the behaviour of the curves is very similar, where the same initial drop is observed, followed by growth to the maximum power value. However, a difference can be observed after the maximum power is obtained. This part of the experiment has a linear behaviour in the time-based normalized power curves, which is not observed in the energy based normalized power curves. This same behaviour is seen in the instantaneous power curves. A difference between instantaneous (Fig. 4) and normalized maximum power (Fig. 5) is also shown. While the peaks of the instantaneous power curves are very close in value, there is a deviation in the value of the peaks of the normalized power. This difference is explained using the average system initial temperature in the normalisation. Due to the design of the tank, which produces temperature inhomogeneities, a small difference may appear between the initial temperatures of the system among the different experiments. This difference is translated to the normalized power curve, causing the curve to shift up or down. If the melting temperature had been taken as the reference temperature, as the methodology in Könnig-Haagen et al. study [17] suggests, this phenomenon would not have been observed. These characteristics are shown in Section 3.1.5. The validation of the instantaneous thermal power come from the discharged energy calculation, which is less than 10% through all the three experiments.

Table 2
Normalized mean power of the three experiments.

Experiment	Normalized power mean value [kW/m^3·K]	
	Time-based ($\overline{\dot{Q}^{norm}_{time}}$)	Energy-based ($\overline{\dot{Q}^{norm}_{energy}}$)
1	3231.98	4889.09
2	2183.59	3706.59
3	1684.68	2812.83

Table 2 shows the normalized energy according to time and energy for the three experiments. This table shows the normalized average power of the tests, calculated using the methodology described in the previous section, seen in both Eq. (10) and Eq. (11). The difference between the tests can be observed, mainly due to the difference observed in the power curves, as these values represent the average power of these curves. On the other hand, it can also be seen that there are differences between normalisation based on time and energy. This difference is to be expected, since the average is calculated based on two different parameters. The normalisation of the average according to time considers the duration of the discharge process, and the normalisation of the average according to energy takes into account the energy discharged.

3.1.5. Normalized discharge power. Melting temperature vs average initial temperature

As mentioned in the previous section, Eq. (9) uses a reference temperature to perform normalisation. This reference temperature can be either the melting temperature or the initial temperature of the system. König-Haagen et al. [17] already describe the differences between taking one temperature or the other as a reference. For example, one advantage of taking the initial temperature rather than the melting temperature is that it considers the boundary conditions in normalisation. However, obtaining this temperature can be complicated, which

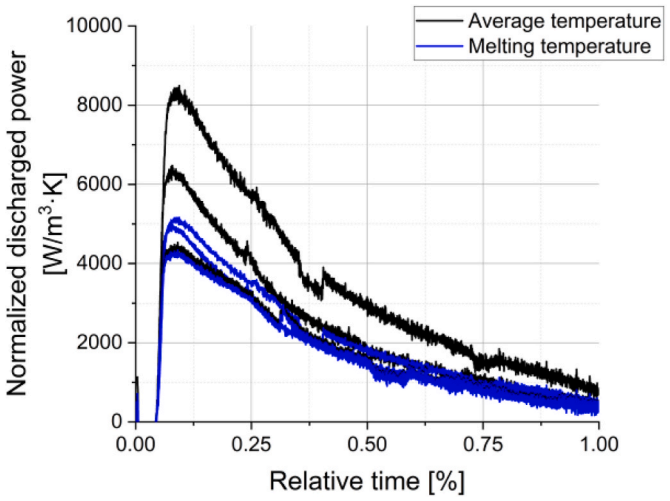

Fig. 6. Normalized discharged power using melting point and average initial temperature for the normalisation procedure.

may result in incorrect normalisation. Fig. 6 shows the difference between the two temperatures. It can be seen that the peak normalized power using the initial temperature of the system is higher than the peak obtained using the phase change temperature, because the difference between the inlet temperature (85 °C) and the melting temperature (92 °C) is greater than the difference between the inlet temperature and the average internal temperature (80, 78 and 77 °C, respectively to experiment 1, 2 and 3). This difference in average temperatures causes a greater difference between the peaks of tests carried out under the same conditions than when using the melting temperature as a reference. This is why the normalized power curves using the melting temperature as a reference are more similar to the instantaneous power curves seen in section 3.1.3.

3.2. IEA SHC Task 58/Annex 33 prototypes

Some of the prototypes used in IEA SHC Task 58/Annex 33 [17] have been selected for the use of normalized power as a methodology for comparing TES systems. Of the eleven different systems proposed, numbers one, four, six and eleven are chosen; but setup number six is only shown in the normalized power vs relative energy plot, as no information of it was found on the normalized power vs relative time plot in the König-Haagen et al. [17] study. Setup number eight was not considered despite showing the highest peak of all the systems presented in the article, showing more than double the power of the next one, setup number 4. Only the curves of the systems whose peaks are close to those of the laboratory prototype have been taken. Setups four, six, one, and eleven, taken for the comparison, have the highest power peaks of all the other prototypes, ruling out setup eight.

Setup number one consists of a cuboid with 72 aluminium capsules filled with magnesium chloride hexahydrate, 250 mm long and 40 mm in diameter [15]. Setup number four consists of a rectangular box measuring 38.75 × 33.7 × 17.75 cm, with 1, 2 or 3 copper coils, filled with dodecanoic acid [42]. Setup number six consists of a cylindrical water tank with a diameter of 0.4 m, with 112 tubes with a diameter of 0.0276 m and a height of 1.52 m, with a composite inside acting as a PCM [43]. Finally, setup number eleven consists of a 1 m^3 tank with hydrated salt and a polypropylene heat exchanger [17].

3.2.1. Normalized thermal power comparison

Fig. 7 shows a comparison between the different IEA SHC Task 58/Annex 33 storage systems [17] and the laboratory prototype.

It can be observed that the maximum normalized power of the laboratory prototype tests is higher than that of setups one, six, and eleven. Setup number four shows a higher power peak, but a very sharp drop in power is also observed in Fig. 7A. This peak is obtained before the other setups reach it in the power vs relative time plot, but Fig. 7B shows that the peak of the setup number four is achieved near the same relative discharged energy as the other setups. It can also be seen that the different IEA SHC Task 58/Annex 33 setups do not start at negative powers or energies, highlighting the need for a better method for

Table 3
Energy capacity, volume, temperature range and system energy density of the studied system and the setups characterized in the Task.[a] System where only the latent heat is accounted for.

System	Energy capacity [kWh]	Total Volume[l]	Temperature range [K]	Energy density [kWh/m^3]
Lab-scale prototype[a]	0.16	13.60	0	11.82
Optimized prototype[a]	0.29	7.08	0	40.83
Task Setup 1	4.56	152	30	30
Task Setup 4	0.78	23.1	21	33.6
Task Setup 6[a]	6.60	282	0	23.64
Task Setup 6	13.89	282	62	46.38
Task Setup 11	14 [44]	1540	0	9.72

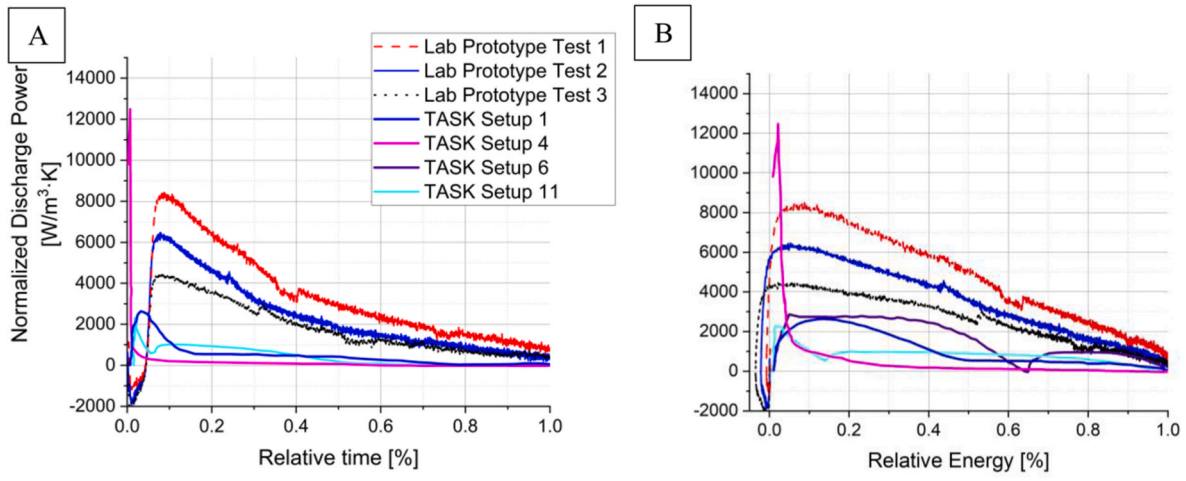

Fig. 7. Normalized discharged power of the lab-scale prototype and the selected setups from the IEA SHC Task 58/Annex 33. A) Normalized discharged power vs. relative time. B) Normalized discharged power vs. relative energy.

calculating system losses. On the other hand, both graphs show that, once the peak power has passed, the prototype system shows the highest normalized power values.

3.2.2. Energy density comparison

Table 3 summarizes the energy densities of the different systems analysed within the IEA SHC Task 58/Annex 33 framework, together with those of the laboratory prototype. Due to the experimental conditions applied in this work (constant inlet temperature), no net sensible energy is stored in the system, as the initial and final temperatures are assumed to be equal. The table also reports the system volumes, stored energy, and operating temperature ranges of the different setups, using the volumes provided by König-Haagen et al. [17].

For Setup 1, the reported energy density is 30 kWh/m^3 with a total volume of 152 L, resulting in a storage capacity of 4.56 kWh [31]. In the case of Setup 4, the reported energy density (56.6 kWh/m^3) is based on the PCM volume (0.01373 m^3). When recalculated using the total system volume derived from the geometric data provided by König-Haagen et al. [17], the energy density decreases to 33.6 kWh/m^3, which is consistent with the range observed in other systems. The corresponding storage capacity is 0.78 kWh.

For Setup 6[a], only long-term storage is considered, assuming that all stored energy corresponds to latent heat, resulting in 24 MJ (6.6 kWh). In contrast, Setup 6 includes both latent and sensible heat contributions, showing an energy density of 46.38 kWh/m^3 and a total storage capacity of 50 MJ (13.89 kWh). An optimized version of Setup 6 is also reported, with an energy density of 72.22 kWh/m^3 for a temperature difference of 62 K. However, when considering only the latent heat contribution, the energy density decreases to 25.86 kWh/m^3. This value is calculated based on the reported total stored energy (81 MJ) and energy density (260 MJ/m^3) of the optimized configuration, corresponding to a system volume of approximately 311 L, with a latent energy contribution of 29 MJ (8.05 kWh). Setup 6[a] is particularly relevant for comparison with the present work, as it also relies on a supercooled PCM. When considering only latent heat storage, Setup 6 exhibits a higher energy density than the laboratory prototype. However, the optimized configuration of the prototype proposed in this study achieves higher energy densities, mainly due to the increased PCM fraction and the reduction of non-active system volume, such as the removal of the jacket, unused in the tests.

Finally, Setup 11 does not appear in the IEA SHC Task 58/Annex 33 report [31], but it is described by König-Haagen et al. [17]. According to Rathgeber et al. [44], the latent heat storage capacity is 14 kWh. Using the system volume reported in König-Haagen et al. [17], this corresponds to an energy density of 9.72 kWh/m^3, the lowest among the analysed systems. It should be noted that this value does not account for sensible heat storage, which could increase its effective energy density and bring it closer to the values reported for Setups 1 and 4.

As expected, energy density is highly dependent on the system's initial and final operating temperatures, even in configurations where the latent heat is the dominant storage mechanism. It is therefore important to clearly define both the temperature range in which the system operates and whether the available energy refers to the latent heat of the PCM or the sensible heat of the PCM and the system.

3.3. Thermal energy storage commercial systems

As discussed in the methodology section, four different commercially available systems are compared to a lab-scale prototype, developed by the authors of the present study. The methodology used to compare storage systems according to the König-Haagen et al. work [17] requires instantaneous power curves, as well as the initial internal temperature and the volume of the PCM and HTF, in order to normalize the power curve and fairly compare different TES systems. However, comparison with commercial systems is complicated, as the data required for this comparison (power curves, volume, inlet and initial temperatures) has not been provided. The comparison between systems will be made mainly on the basis of energy density and cost per unit of stored energy. However, the reference data for calculating the stored energy or volume is not always explicitly stated in the system data sheet.

Fig. 8. Sunamp Thermino 150 Xplus [37], [45].

The laboratory-scale prototype is not well optimized for a TES system, and improvements could be made in energy density or thermal power, such as improved coil design or filling the tank completely. As mentioned in Section 3.1.1, the optimized lab-scale prototype could store 0.3 kWh of energy in a system of 7.08 L, so the energy density of the optimized system is 40.83 kWh.

3.3.1. Sunamp

Sunamp [37] is a company located in East Lothian, Scotland, and has been active since 2005. Sunamp specializes mainly on hot water systems for residential applications. The company has developed two primary product lines: the Thermino ePlus series and the Thermino xPlus series, both designed for hot water production. The Thermino ePlus only allows for electrical connection, both from the grid and distributed generation. The Thermino xPlus also allows for the connection of a heat pump and a conventional boiler. Additionally, Sunamp is currently developing the Central Bank system, which can work for both hot water and heating applications. For the comparison, only the Thermino xPlus series is considered.

The Thermino 150xPlus model, shown in Fig. 8, weights 136 kg and its dimensions are 0.365m width x 0.575m depth x 0.64m height, with a total volume of 0.134 m^3. The draw-off volume (V40) is 167 l. Assuming a temperature difference of 30 K (from 40 °C to 10 °C), the energy available is 5.81 kWh. As the volume is 0.134 m^3 and the available energy is 5.81 kWh, the energy density is 43.35 kWh/m^3. The recommended working temperature is 45-55 °C, and a flow rate of 15 l/min. Its thermal losses are 0.67 kWh/24 h, or 28.1 W. The system costs 1950€ [45], making the price per unit of energy 335€/kWh.

Plentigrade serves as the phase change material used in the thermal energy system. To improve the performance and prevent phase segregation, sodium acetate trihydrate is mixed with Na-PMAA polymer (to prevent phase segregation), and Na_2HPO_4-$2H_2O$ salt to activate

Fig. 9. Cowa Thermal solution technology. A) Macroencapsulated PCM [49]. B) Cowa Compact Cell 58 [38].

crystallization [46]. Different melting points (−30 °C, 5 °C, 58 °C, 118 °C) are available for the different storage systems. Sodium acetate trihydrate has a phase change enthalpy of 264 J/g, and a density of 1530 kg/m^3, resulting in an energy density of 112 kWh/m^3 [47], [48].

Using the latent heat of 264 kJ/kg, the energy available of 5.81 kWh, and all the energy stored is due to the phase change of the Plentigrade, the total mass of the Plentigrade used is 79.2 kg; making the pipes, insulation and other components a total of 56.8 kg.

3.3.2. *Cowa Thermal Solutions*

Cowa [38] is a spin-off of the University of Lucerne, specialising in domestic hot water and heating solutions. The storage system works with an external heat pump. The heat is generated by this heat pump, which they also supply.

The Compact cell 58, which can function as a buffer system or as a domestic hot water cylinder, is the system selected for this work. Cowa also offers the Compact Cell 48/58 combi, which integrates a domestic hot water and heating buffer cylinder in a compact solution, shown in Fig. 9B.

The Compact Cell 58 wt 250 kg, and its dimensions are 0.6m width x 0.34m depth x 1.4m height, making a total volume of 0.285 m^3 (285 l). The draw-off volume (V40) is 380 l, which, assuming a temperature difference of 30 K, translates to an available energy of 13.23 kWh, very similar to the storage capacity indicated in the data sheet. As the storage capacity is 13.23 kWh, and the total volume is 0.285 m^3, the energy density of the system is 46.42 kWh/m^3. This energy density is lower than 75 kWh/m^3, the energy density specified in the data sheet.

The Compact Cell 58 system uses the Cowa 58 PCM, a salt hydrate-based phase change material. Its enthalpy is 260 kJ/kg, and its density is 1460 kg/m^3. Its energy density is 107 kWh/m^3. The PCM is encapsulated in a plastic container, as shown in Fig. 9A.

Using the phase change enthalpy of 260 J/g, and all the energy stored is due to the phase change of the Cowa 58PCM, the mass of the PCM in the system is 183.2 kg, making the pipes, insulation and other components a total of 66.8 kg. The working temperature of the system is 48-58 °C, and the thermal power goes up to 20 kW. The possible water flow is 25 l/min. The price of the system is 4500€.

3.3.3. *Kraftboxx*

Kraftboxx [39] is a German company that supplies both the kraftBoxx and heatBoxx products. Both systems use macro-encapsulation

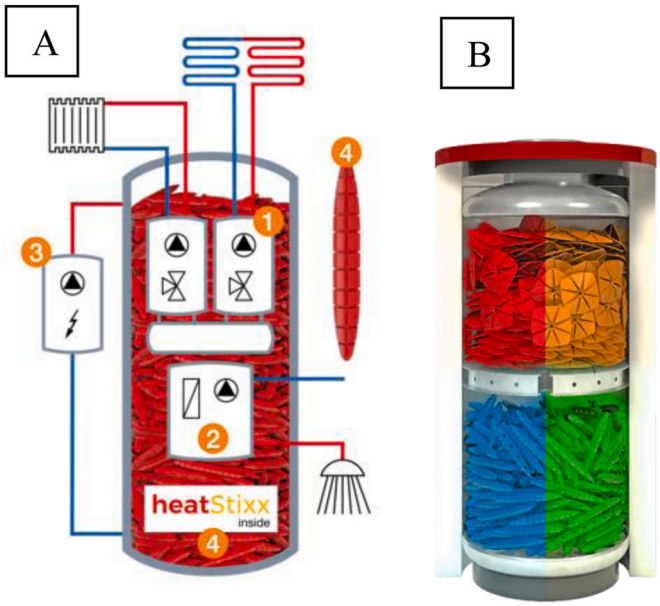

Fig. 10. Kraftboxx TES system. A) Scheme of the different applications of the systems. B) Kraftboxx system with of the HeatStixx and HeatSel macro-encapsulation [39].

within a tank for energy storage, specifically the heatSel and heatStixxL, found in Fig. 10B. The system selected for this work is the krafftBoxx product.

The energy storage capacity and phase change characteristics are dependent on the selected phase change material. Although different PCMs are available for this application, the system characteristics data provided by the supplier corresponds to characteristics of the system using the ATS 50, a PCM with a phase change temperature of 50 °C and a phase change enthalpy of 230 kJ/kg, corresponding to an energy density of 39 kWh/m^3 when it is encapsulated inside the heatStixxL.

For the case of the Kraftboxx 1000, the used macroencapsulated is only the heatStixxL. This system has a diameter of 0.79 m and a height of 2.044 m, which translates to a volume of 1.001 m^3. The insulation used

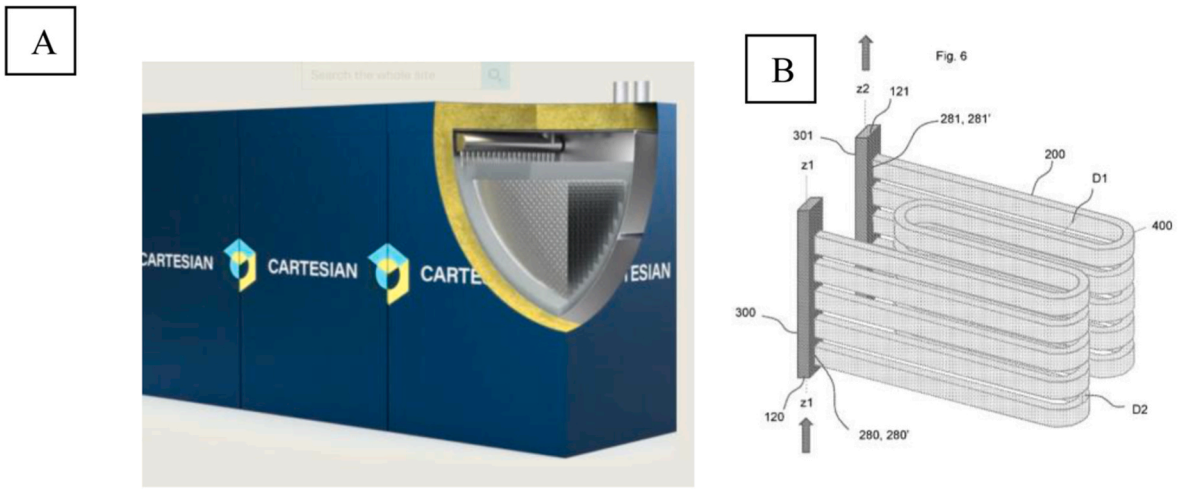

Fig. 11. Cartesian TES system. A) Commercial system B) Picture of the heat exchanger used in the energy storage system [40], [50], [51].

Table 4
Comparison between xylitol and different commercial PCMs.

Material	Company	Type	Melting Temperature [°C]	Energy density [kWh/m^3]	Enthalpy [kJ/kg]
Xylitol	University of Zaragoza	Sugar Alcohol	92	97	240
Plentigrade	Sunamp	Hydrated salt	58	112	260
ATS 50	Krafftboxx	Inorganic (not specified)	50	82	228
Cowa PCM 58	Cowa	Hydrated salt	58	136	260
Cartesian PCM	Cartesian	Biobased Wax	74	—	—

has a thickness of 10 cm. However, it is not specified if the insulation is included in the diameter of the system or not. If it is not included in the diameter of the system, the total volume changes to 1.573 m^3.

The energy capacity is reported as 42 kWh for the 1000 l configuration. Each heatStixxL has a diameter of 0.035m and a length of 0.26m, so each heatStixxL has a volume of 0.00025 m^3. The number of HeatStixxL for each tank is 900, so the energy available should be 19.56 kWh (900 pieces · 0.00025m^3/piece · 42 kWh/m^3), much lower than the 42 kWh reported. Using the phase change enthalpy of the ATS50 (313 kJ/l), assuming all volume is PCM; and 2000 pieces per tank, as stated by the heatStixxL datasheet of 200 pieces per 100 l, the total energy stored is 43.47 kWh (2000 pieces · 0.25L/piece · 313 kJ/L), the energy capacity reported in the krafftBoxx datasheet.

The system's load is directly supplied by an external hot water source, like a heat pump or a water boiler. Fig. 10A shows the scheme of the Krafftbox product. The tank price is 2660€, and each heatStixxL cost 4.49€. If the heatStixxL is included, the price of the system (tank + PCM) is 6701€ (900 pieces) or 11640€ (2000 pieces).

3.3.4. Cartesian

Cartesian is a Norwegian company that uses phase change materials for energy storage. The company specifies that it can work with a very wide temperature range, by adapting the material, from −20 to 120 °C. Their system incorporates a customized coiled heat exchanger, shown in Fig. 11B.

The product offered, known as the Thermal Box (Fig. 11A), can store up to 75 kWh of energy, with dimensions measuring 1.4 m × 1.0 m x 2.0 m (volume of 2.8 m^3) with insulation, resulting in an energy density of 26.78 kWh/m^3. The thermal power of this system goes from 5 to 20 kW, and the working temperature of the system ranges from 60 to 80 ^{0}C for the heating system. Additionally, they have developed a procedure to check the state of charge of the material by using a wave property. The thermal losses of the system are reported to be 1%/24 h, and the maximum heat transfer fluid flow rate is 6 m^3/h.

A bio-based wax is used as PCM in this system. This wax has a phase change temperature of 74 ^{0}C, but no more data on this PCM was found.

3.3.5. Comparison of the energy storage material and system

The comparison is two-fold. Table 4 shows the comparison between the materials used in the systems, and Table 4 shows the comparison between the systems themselves. As not all the information is available, some cells of the table are left as blanks. Since it has not been possible to access the power curve data for the systems, the comparison between the prototype system and commercial systems is not made using the methodology shown in Section 2.2.3, but other parameters will be used for this comparison. As commercial systems do provide data on the energy density of the system, this variable will be considered for comparison purposes. In the case of the laboratory prototype, the IEA SHC Task 58/Annex 33 definition for system energy density will be used, taking the total volume of the system, including insulation, as the volume for the energy density calculation (Eq. (6)).

For the comparison of systems in Table 3, both the laboratory prototype system and an optimized laboratory prototype system are compared with a theoretical commercial system, calculated using commercial prices. As mentioned at the beginning of section 3.3, the optimized laboratory prototype has a volume of 7.08 L and can store 0.3 kWh of energy, giving it an energy density of 40.8 kWh/m^3. Using commercial prices, the cost of this system is close to 500€, making its cost per unit of energy around 1500€/kWh. On the other hand, for the theoretical commercial system, a commercial tank with a 750l internal volume (1.4 m^3 external volume) with one coil, filled entirely with xylitol, has been assumed. This storage system could store around 69.5 kWh, giving it an energy density of 49.2 kWh/m^3. Furthermore, its price is estimated to be close to 15000€, so the cost per unit of energy is estimated at 216€/kWh.

Table 4 shows that xylitol is a very promising material. Its energy density is similar to the Plentigrade and the Cowa 58PCM, but the melting point is higher than the intended melting point of these two materials (92 °C vs 58 °C). However, the melting point of 92 °C can work correctly with both domestic hot water and heating applications. Additionally, xylitol does not suffer from phase segregation, but it does suffer from supercooling and a low crystallization rate, which is why a

Table 5
Comparison between lab scale prototype and commercially available solutions.

System	Company	Material	Working temperature [°C]	Energy density [kWh/m^3]	System Energy capacity [kWh]	Volume [L]	Thermal Power [kW]	Energy losses	Price [€/kWh]
Stirred Tank	University of Zaragoza	Xylitol	70-100	11.85	0.16	13.6	—	—	16875
Optimized Stirred Tank	University of Zaragoza	Xylitol	70-100	40.83	0.29	7.08	—	—	1500
Theoretical commercial tank	University of Zaragoza	Xylitol	70-100	49.2	69.5	750	—	—	216
Termino 150xPlus	Sunamp	Plentigrade	45-55	43.35	5.81	134	—	0.67 kWh/24 h	335
Cowa Compact cell 58	Cowa	Cowa 58 PCM	55	46.42	13.23	285	20	—	340
Kraftboxx 1000	Krafftboxx	HeatSel with ATS50	50	42	42	1000	—	—	330
Thermal Box	Cartesian	Bio-based wax	60-80	27	75	2800	20	1%/24 h	—

stirrer with seeding is needed.

Plentigrade and Cowa 58PCM shows very similar characteristics, while the ATS50 show lower energy density than both of them and xylitol. All the commercially available materials are inorganic materials, while xylitol is an organic material.

Table 5 shows the comparison between the systems. The lowest energy capacity per unit of volume is shown in the Cartesian Thermal Box product. Surprisingly, the kraftBoxx product show a high energy capacity, even though the material used has a lower energy density than the material used in the Thermino xPlus or the Cowa Compact Cell 58. The lab scale prototype shows four times less energy density, as it has not been optimized. The optimized stirred tank is cheaper than the actual tank, and it shows a similar energy density than the commercial systems.

4. Conclusions

The main objective of this work is the benchmarking of a xylitol-based TES prototype to different TES solutions that can operate under similar temperature and power conditions. To do so, this study evaluates the potential of a xylitol-based TES prototype, with the shearing and seeding technique to promote the thermal energy discharge, with an internal helical coil as heat exchanger. This evaluation has been made according to the characterization methodology proposed by the IEA SHC Task 58/Annex 33, in terms of energy density and thermal power. The energy density of the lab scale prototype is 11.85 kWh/m^3 taking into account the insulation and 18.04 kWh/m^3 for the no insulation case.

Regarding the normalized thermal power, the prototype behaves similarly to the IEA SHC Task 58/Annex 33 prototypes. Its thermal power is higher than that of the other selected prototypes throughout the tests, although one of the setups shows a higher peak power than the prototype in this study. However, this setup shows a very sharp drop in thermal power, which causes the xylitol-based prototype to become the TES system with the highest normalized thermal power through the rest of the experiment.

To assess its competitiveness, it has been compared to current commercial solutions. These commercial solutions include the Cowa compact cell 58, the Sunamp Thermino 150XPlus and the KrafftBoxx 1000L. All three show very similar energy densities and price per unit of energy, even though the energy capacity is different between them. The Cartesian Thermal box shows the lowest energy density while being the largest TES system. It should be noted that these commercial solutions cannot be fully evaluated according to the methodology because there is no standardisation of the parameters and information provided by the systems.

In contrast, the current prototype reached a lower energy density than the commercial solutions. The difference is primarily attributed to its non-optimized design of the laboratory prototype. The analysis of an optimized system configuration, where xylitol occupies the entire available internal volume and only the coil is used as a temperature control system, projects an energy density of up to 40.8 kWh/m^3. This value positions xylitol-based technology within the same performance range as market solutions, confirming its high potential for medium-low temperature applications. A theoretical commercial stirred tank system with xylitol could be compared to commercial storage systems, having a higher energy density (49.2 kWh/m^3) and lower cost per unit of energy.

Finally, a highlight of this work is the identification of a gap between academic methodologies and industrial practices in the characterization of thermal energy storage systems. While standardized frameworks are already found in literature, such as those proposed by the IEA SHC Task 58, their practical application to commercially available systems remain limited due to the lack of sufficiently detailed and transparent data. This mismatch hinders fair benchmarking and may lead to misleading comparisons between laboratory-scale prototypes and industrial solutions.

CRediT authorship contribution statement

Miguel Navarro: Writing – review & editing, Writing – original draft, Visualization, Validation, Supervision, Software, Resources, Project administration, Methodology, Investigation, Funding acquisition, Formal analysis, Data curation, Conceptualization. **Ana Lázaro:** Writing – review & editing, Writing – original draft, Visualization, Validation, Supervision, Resources, Project administration, Methodology, Investigation, Funding acquisition, Formal analysis, Conceptualization. **Mónica Delgado:** Writing – review & editing, Writing – original draft, Visualization, Validation, Supervision, Resources, Project administration, Methodology, Investigation, Funding acquisition, Formal analysis, Conceptualization.

Declaration of competing interest

The authors declare that they have no known competing financial interests or personal relationships that could have appeared to influence the work reported in this paper.

Acknowledgments

This work has been partially financed by the State Research Agency (SRA) and European Regional Development Fund (ERDF). Research Project: PID2023-148958OB-C21 and Grant PRE2021-097131 funded by MICIU/AEI/ 10.13039/501100011033 and, as appropriate, by "ERDF A way of making Europe", by "ERDF/EU", by the "European Union" or by the "European Union Next Generation EU/PRTR" with the additional support of the government of Aragon (Spain) (Reference group T55_23 R). Mónica Delgado thanks grant RYC2023-044207-I funded by MICIU/AEI/10.13039/501100011033 and the European

Social Fund Plus.

Data availability

Data will be made available on request.

References

[1] Mofijur M, et al. Phase Change Materials (PCM) for solar energy usages and storage: an overview. Energies ago. 2019;12(16):3167. https://doi.org/10.3390/en12163167.

[2] Chavan S, Rudrapati R, Manickam y S. A comprehensive review on current advances of thermal energy storage and its applications. Alex Eng J jul. 2022;61(n.o 7):5455–63. https://doi.org/10.1016/j.aej.2021.11.003.

[3] Hurst K, et al. «Industrial energy storage review». Golden, CO (United States): National Renewable Energy Laboratory (NREL); oct. 2024. https://doi.org/10.2172/2473658.

[4] Carrillo AJ, González-Aguilar J, Romero M, Coronado y JM. Solar energy on demand: a review on high temperature thermochemical heat storage systems and materials. Chem Rev 2019;119(7). https://doi.org/10.1021/acs.chemrev.8b00315. 4777-4816, abr.

[5] Zalba B, Marín JM, Ma Marin Jose, Cabeza LF, Mehling y H. Review on thermal energy storage with phase change: materials, heat transfer analysis and applications. Appl Therm Eng feb. 2003;23(n.o 3):251–83. https://doi.org/10.1016/s1359-4311(02)00192-8.

[6] Chaturvedi R, Islam A, Sharma y K. A review on the applications of PCM in thermal storage of solar energy. Mater Today Proc 2021;43:293–7. https://doi.org/10.1016/j.matpr.2020.11.665.

[7] Sarbu I, Sarbu Ioan, Dorca y A. Review on heat transfer analysis in thermal energy storage using latent heat storage systems and phase change materials. Int J Energy Res ene. 2019;43(n.o 1):29–64. https://doi.org/10.1002/er.4196.

[8] Larrinaga P, Diarce G, Campos-Celador Á, García-Romero y A. Parametric characterization of a full-scale plate-based latent heat thermal energy storage system. Appl Therm Eng sep. 2020;178:115441. https://doi.org/10.1016/j.applthermaleng.2020.115441.

[9] Dolado P, Lazaro A, Marin JM, Zalba y B. Characterization of melting and solidification in a real scale PCM-air heat exchanger: numerical model and experimental validation. Energy Convers Manag abr. 2011;52(n.o 4):1890–907. https://doi.org/10.1016/j.enconman.2010.11.017.

[10] Rinaldi G, Lazaro A, Delgado M, Marin JM, Verda y V. Use of a low-cost phase change material emulsion in de-centralized thermal energy storage for district heating network enlargement. Energy oct. 2024;306:132517. https://doi.org/10.1016/j.energy.2024.132517.

[11] Delgado M, Lázaro A, Mazo J, Peñalosa C, Dolado P, Zalba y B. Experimental analysis of a low cost phase change material emulsion for its use as thermal storage system. Energy Convers Manag dic. 2015;106:201–12. https://doi.org/10.1016/j.enconman.2015.09.033.

[12] Luo M, Zhang Y, Nie Y, Lu B, Liu S, Luo y J. Experimental investigation on the thermal performance of a pilot-scale single-tank high-temperature molten salt sensible thermal energy storage system. Energy 2026;342:139686. https://doi.org/10.1016/j.energy.2025.139686. ene.

[13] Yang Sheng, Shao Xue-Feng, Luo Jia-Hao, Oskouei Seyedmohsen Baghaei, Bayer Özgür, Fan y Li-Wu. «A novel cascade latent heat thermal energy storage system consisting of erythritol and paraffin wax for deep recovery of medium-temperature industrial waste heat». Energy 2022. https://doi.org/10.1016/j.energy.2022.126359.

[14] Zondag HA, De Boer R, Smeding SF, Van Der Kamp y J. Performance analysis of industrial PCM heat storage lab prototype. J Energy Storage ago. 2018;18:402–13. https://doi.org/10.1016/j.est.2018.05.007.

[15] Brüggemann D, et al. «Entwicklung makroverkapselter Latentwärmespeicher für den Transport von Abwärme (MALATrans) : Abschlussbericht : Laufzeit: 01.07.2013. bis 31.12.2016».

[16] Pinnau S. Strömungs- und kältetechnische Optimierung von Latentkältespeichern: Abschlussbericht. Technische Univ.; 2009 [En línea]. Disponible en: https://books.google.es/books?id=LCd40AEACAAJ.

[17] König-Haagen A, et al. Analysis of the discharging process of latent heat thermal energy storage units by means of normalized power parameters. J Energy Storage nov. 2023;72:108428. https://doi.org/10.1016/j.est.2023.108428.

[18] Lazaro A, Delgado M, König-Haagen A, Höhlein S, Diarce y G. «Technical Performance Assessment of Phase Change Material Components», en *Proceedings of the ISES Solar World Congress 2019*, Santiago, Chile. International Solar Energy Society 2019:1–12. https://doi.org/10.18086/swc.2019.22.05.

[19] Del Barrio EP, Cadoret R, Daranlot J, Achchaq y F. New sugar alcohols mixtures for long-term thermal energy storage applications at temperatures between 70 °C and 100 °C. Sol Energy Mater Sol Cell oct. 2016;155:454–68. https://doi.org/10.1016/j.solmat.2016.06.048.

[20] Diarce G, Gandarias I, Campos-Celador Á, García-Romero A, Griesser y UJ. Eutectic mixtures of sugar alcohols for thermal energy storage in the 50–90°C temperature range. Sol Energy Mater Sol Cell mar. 2015;134:215–26. https://doi.org/10.1016/j.solmat.2014.11.050.

[21] Zhang HH, et al. Experimental and in silico characterization of xylitol as seasonal heat storage material. Fluid Phase Equilib mar. 2017;436:55–68. https://doi.org/10.1016/j.fluid.2016.12.020.

[22] Xue-Feng Shao et al., «Screening of sugar alcohols and their binary eutectic mixtures as phase change materials for low-to-medium temperature thermal energy storage. (II): Isothermal milting and crystallization behaviors», Energy, doi: 10.1016/j.energy.2019.05.109.

[23] Xuefeng S, et al. Screening of sugar alcohols and their binary eutectic mixtures as phase change materials for low-to-medium temperature thermal energy storage. (III): thermal endurance. Energy oct. 2020;209:118483. https://doi.org/10.1016/j.energy.2020.118483.

[24] Shao X, Chen X, Zhang Y, Lü X, Yuan y Y. Polyalcohols for flexible thermal energy storage: understanding persistent supercooling from Gibbs free energy. Energy sep. 2025;330:136942. https://doi.org/10.1016/j.energy.2025.136942.

[25] Delgado M, Navarro MAE, Lázaro A, Boyer SAE, Peuvrel-Disdier Edith, Peuvrel-Disdier y E. Triggering and acceleration of xylitol crystallization by seeding and shearing: Rheo-optical and rheological investigation. Sol Energy Mater Sol Cell 2021;220:110840. https://doi.org/10.1016/j.solmat.2020.110840.

[26] Navarro M, Gracia Z, Asín J, Lázaro A, Martí M, Delgado y M. Rheological study on xylitol crystallization for its use as phase change material: analytical and statistical analysis. Sol Energy Mater Sol Cell oct. 2025;292:113803. https://doi.org/10.1016/j.solmat.2025.113803.

[27] Piquard Louis, Gagnière Emilie, Largiller Grégory, Mangin Denis, Bentivoglio y F. Xylitol used as phase change material: nucleation mechanisms of the supercooling rupture by stirring. J Energy Storage abr. 2022;48. https://doi.org/10.1016/j.est.2021.103922. 103922-103922.

[28] Piquard L, Gagnière É, Largiller G, Mangin D, Bentivoglio y F. Triggering Xylitol crystallization in a 42 kWhth shell and tubes latent heat thermal energy storage system. Appl Therm Eng 2022. https://doi.org/10.1016/j.applthermaleng.2022.119802.

[29] Anish R, Mariappan V, Suresh S, Joybari MM, Abdulateef y AM. Experimental investigation on the energy storage/discharge performance of xylitol in a compact spiral coil heat exchanger. Int J Therm Sci 2021;159:106633. https://doi.org/10.1016/j.ijthermalsci.2020.106633. ene.

[30] Navarro M, Diarce G, Lázaro A, Rojo A, Delgado y M. Comparative study on bubbling and shearing techniques for the crystallization of xylitol in TES systems. Results Eng mar. 2023;17:100909. https://doi.org/10.1016/j.rineng.2023.100909.

[31] Van Helden A Hauer y W. «MATERIAL AND COMPONENT DEVELOPMENT FOR THERMAL ENERGY STORAGE», SHC Task 58/ECES Annex 33, Final Report. Accedido: 28 de enero de [En línea]. Disponible en: https://iea-es.org/wp-content/uploads/public/IEA-ES-TCP-Annex-33-Final-Report_revised-May-2021.pdf; 2026.

[32] Tomassetti S, et al. A review on thermophysical properties and thermal stability of sugar alcohols as phase change materials. J Energy Storage nov. 2022;55:105456. https://doi.org/10.1016/j.est.2022.105456.

[33] King AM Omran y CJ. Kinetics of ice crystallization in sugar solutions and fruit juices. AIChE J jul. 1974;20(n.o 4):795–803. https://doi.org/10.1002/aic.690200422.

[34] Myerson AS, Erdemir D, Lee y AY, editors. Handbook of industrial crystallization, 3.a. Cambridge University Press; 2019. https://doi.org/10.1017/9781139026949.

[35] Shao X, Yang S, Fan L, Yuan y Y. Sugar alcohol phase change materials for low-to-medium temperature thermal energy storage: a comprehensive review. J Energy Storage sep. 2023;68:107848. https://doi.org/10.1016/j.est.2023.107848.

[36] del Barrio EP, et al. Characterization of different sugar alcohols as phase change materials for thermal energy storage applications. Sol Energy Mater Sol Cell ene. 2017;159:560–9. https://doi.org/10.1016/j.solmat.2016.10.009.

[37] «Sunamp Website». Accedido: 23 de julio de 2025 [En línea]. Disponible en: https://sunamp.com/es/.

[38] Cowa Thermal solutions Website». Accedido: 23 de julio de [En línea]. Disponible en: https://www.cowa-ts.com/en/products/domestic-hot-water; 2025.

[39] «Kraftboxx Website». Accedido: 23 de julio de 2025 [En línea]. Disponible en: https://heatstixx.de/.

[40] «Cartesian Website». Accedido: 23 de julio de 2025 [En línea]. Disponible en: https://cartesian.no/.

[41] Cabeza H Mehling y LF. Heat and cold storage with PCM: an up to date introduction into basics and applications. en Heat and Mass Transfer. Berlin, Heidelberg: Springer Berlin Heidelberg; 2008. https://doi.org/10.1007/978-3-540-68557-9.

[42] Patil A. Experimental study of coil and shell phase change material heat exchanger. Halifax, Canada: Dalhousie University; 2020.

[43] Wang G, Dannemand M, Xu C, Englmair G, Furbo S, Fan y J. Thermal characteristics of a long-term heat storage unit with sodium acetate trihydrate. Appl Therm Eng mar. 2021;187:116563. https://doi.org/10.1016/j.applthermaleng.2021.116563.

[44] Rathgeber C, Helm M, Hiebler y S. Energy storage for the energy transition: Salt hydrate based low-temperature latent heat storage. Chem Ing Tech ene. 2018;90(1–2):193–200. https://doi.org/10.1002/cite.201700049.

[45] «Sunamp Shop». Accedido: 27 de enero de 2026 [En línea]. Disponible en: https://sunamp.shop/products/sunamp-thermino-150epv.

[46] Oliver DE, Bissell AJ, Liu X, Tang CC, Pulham y CR. Crystallisation studies of sodium acetate trihydrate – suppression of incongruent melting and sub-cooling to produce a reliable, high-performance phase-change material. CrystEngComm 2021;23(o 3):700–6. https://doi.org/10.1039/D0CE01454K.

[47] Englmair G, Moser C, Furbo S, Dannemand M, Fan y J. Design and functionality of a segmented heat-storage prototype utilizing stable supercooling of sodium acetate trihydrate in a solar heating system. Appl Energy jul. 2018;221:522–34. https://doi.org/10.1016/j.apenergy.2018.03.124.

[48] Dannemand M, Schultz JM, Johansen JB, Furbo y S. Long term thermal energy storage with stable supercooled sodium acetate trihydrate. Appl Therm Eng dic. 2015;91:671–8. https://doi.org/10.1016/j.applthermaleng.2015.08.055.
[49] Miranda S. New generation of thermal energy storages. Accedido; 27 de enero de 2026 [En línea]. Disponible en: https://www.hslu.ch/-/media/campus/common/files/dokumente/ta/ta-forschung/tes/sstes24-referats/sstes-24-simon-maranda-cowa-new-generation-of-thermal-energy-storage.pdf.
[50] A. Sevault, O. Galteland, M. Rotan, R. SAEterli, y F. Vallum-Bruer, «Procédé et système de commande d'état de charge de systèmes de stockage de matériau à changement de phase», PCT/NO2024/050037.
[51] A. Sevault, «Système de stockage d'énergie thermique», PCT/NO2023/050125.